Pergamon

Planet. Space Sci., Vol. 43, No. 9, pp. 1135–1146, 1995

0032–0633/95 $9.50+0.00

0032–0633(95)00038–0

Comparative study of numerical simulations of the solar wind interaction with Venus

T. K. Breus,[1] A. M. Krymskii[2] and V. Ya. Mitnitskii[3]

[1] Space Research Institute, Profsoyuznaya 84/32, 117810 Moscow, Russia
[2] Rostov State University, Rostov-on Don, Russia
[3] Computer Centre, Russian Academy of Sciences, Moscow, Russia

Received 1 December 1993; revised 20 December 1994; accepted 28 January 1995

Abstract. The assumptions and peculiarities of the numerical codes, as well as the spatial resolution of the gas-dynamical and hybrid simulations which are available at present are discussed. As found the present day estimates of O^+ ion production rates which can effect the bow shock geometry as intensively as observed by *Pioneer-Venus-Orbiter* are controversial. The disagreement of the gas-dynamical simulations by Breus *et al.* (*Planet. Space Sci.* **40**, 131–138, 1992) and Stahara and Spreiter (*Venus and Mars*: *Atmospheres, Ionospheres and Solar Wind Interactions*, Geophysical Monograph 66, p. 345. AGU, 1992) is a result of different numerical implementation of the flow tangency condition which does not permit the specification of the equation of state $p = p(\rho)$ at the impenetrable obstacle. The numerical code by Breus *et al.* uses the reflection procedure for the implementation of the flow tangency condition and is insensitive to the equation of state at the obstacle surface. The reflection procedure does not employ explicitly the boundary conditions at the obstacle which the Stahara and Spreiter code does. As a result Stahara and Spreiter's (*Venus and Mars*: *Atmospheres, Ionospheres and Solar Wind Interactions*, Geophysical Monograph 66, p. 345. AGU, 1992) simulation is in agreement with observations only in the case of an unreasonable value of the electron impact ionization: in several times of the photoionization within the magnetic barrier at Venus. Breus *et al.* (*Planet. Space Sci.* **40**, 131–138, 1992) agree well with observations if the electron impact ionization is 60–70% of the photoionization there. Brecht and Ferrante (*J. geophys. Res.* **96**, 11209–11220, 1991) simulated an insignificant effect of the magnetic barrier on the shock geometry. However this simulation is unable to estimate the O^+ ionization rate to fit the hybrid model with observations. The cells employed by Moore *et al.* (*J. geophys. Res.* **96**, 7779–7791, 1991) are larger than the thickness of the magnetic barrier region estimated from the magnetometer data by Zhang *et al.* (*J. geophys. Res.* **96**, 11145–11153, 1991). Thus Moore *et al.* cannot simulate the magnetic barrier region properly and their prediction of an insignificant effect of the mass-loading under any expectable O^+ ion production rate should be revised.

1. Introduction

Numerical simulations of the solar wind interaction with planets have a rather long history. A numerical code describing the interaction of a blunt body in a supersonic flow was originally developed and successfully applied by Spreiter *et al.* (1966) to the solar wind interaction with the Earth. The actual bow shock position was simulated on the basis that the magnetopause, surrounding the magnetosphere was an impenetrable obstacle to the solar wind flow. Later the same gas dynamic (GD) code was applied to the simulation of the solar wind interaction with planetary ionospheres (Spreiter *et al.*, 1970). Here the ionopause is treated as an impenetrable obstacle at the "non-magnetic" planets Venus and Mars. A decade later the results of the numerical simulations are still of interest and of value (Spreiter and Stahara, 1980a,b). The *Pioneer-Venus-Orbiter* (PVO), on orbit around Venus, with its bow shock crossing and subsequent passes through the ionosphere region on the same orbit provides a unique opportunity for comparison of GD simulations with *in-situ* data. Mihalov *et al.* (1982) compared such data obtained at specially selected orbits (No. 582 and 129) during steady state solar wind conditions with results obtained from GD simulations based on the values of GD parameters, estimated using experimental data, such as ambient solar wind Mach number or the shape of the obstacle defined by the shape of the ionopause. However, the bow shock positions obtained in such simulations were located substantially closer to the planet than the actually measured positions of the shock front.

Correspondence to: T. K. Breus

At least two effects which were overlooked by the initial GD code of Spreiter and Stahara can be expected to increase the distance of the bow shock at Venus: (1) deceleration of the solar wind flow near the planet due to pick-up of new-born heavy ions (mass-loading); (2) the pile-up of the interplanetary magnetic field (IMF) around the impenetrable obstacle (magnetic barrier) which effectively deflects some part of the solar wind flow.

Despite rather extended numerical simulations the magnitude of the mass-loading effect on the bow shock as well as the magnetic barrier effect are still controversial. As a consequence the validity of the GD numerical simulations of the SW interaction with a non-magnetic (or weakly magnetized) planet and the effect of the mass-loading on the global interaction pattern have been questioned. Belotserkovskii *et al.* (1987) in their GD model took into account the photoionization of neutral oxygen corona at Venus. They predicted the position of the bow shock closer to the actual PVO shock crossing during orbit 582 by virtue of prescribing the empirical altitude profile of the neutral oxygen density and the actual value of the ambient solar wind Mach number. Later Stahara *et al.* (1987) reported no substantial effect of the mass-loading on the bow shock position. In Stahara *et al.*'s (1987) model all parameters were identical to those used by Belotserkovskii *et al.* (1987). This casts serious doubts on both the magnitude of the mass-loading as estimated by Belotserkovskii *et al.* (1987) and their numerical algorithm.

The principal problems of the GD simulation of the solar wind interaction with Venus were examined by Breus and Krymskii (1992). The arguments for the fluid-like behaviour of plasma throughout the interaction region at Venus were presented. Recently a new two-fluid GD model for the solar wind interaction with Venus and Mars was developed by Breus *et al.* (1992) independent of the previous one-fluid GD model by Belotserkovskii *et al.* (1987). When the numerical simulations by Belotserkovskii *et al.* (1987) and Breus *et al.* (1992) were compared it became clear that the simulations by Breus *et al.* (1992) gave the bow shock at $2.2R_0$ (R_0 is the subsolar obstacle distance from the planetary centre) or $2.31R_v$ (R_v is the Venus radius) within the terminator plane. On the other hand Belotserkovskii *et al.* reported: $2.4R_0$ and $2.5R_v$, respectively. As became obvious later, Belotserkovskii *et al.* (1987) interrupted their computational run before the solution converged. The results by Breus *et al.* (1992) are intermediate between the results of Belotserkovskii *et al.* (1987) and Stahara *et al.* (1987), and the mass-loading effect increases the distance of the bow shock nevertheless by 10% in comparison to the model which does not take into account the mass-loading. Thus the contradiction among the GD model (including mass-loading) still remains.

Critics of the GD approach state that the magnetic field effects (magnetic barrier formation, finite ion gyroradii) are not properly taken into account by the GD approach. To study the magnetic barrier effects MHD theory or a hybrid model of the plasma have to be used. Both approaches treat the plasma electrons as a fluid. In MHD theory the ions are also treated as a fluid-like, whereas in the hybrid model the ions are in a kinetic fashion. The magnetic field is frozen into the electron fluid: the Hall electric field is responsible for the deflection of the solar wind flow by the magnetic barrier. It depends on the electron thermal pressure and the Lorentz force in both approaches. To be more precise the Hall electric field is independent of grad p_e but we have combined it with "ambipolar" electric field grad p_e/en for the sake of simplicity.

Hybrid models have some advantages over MHD models, however they require very intensive computational efforts. To make computational runs possible some extra assumptions are employed. The fine spatial resolution in the vicinity of the body is required for adequate simulations. Simulations with poor resolution are open to incorrect interpretation (Brecht and Ferrante, 1991). Only detailed comparison of all presently available models (GD, MHD and hybrid models) of the solar wind interaction with Venus can identify the various problems and limitations of these models.

Brecht and Ferrante (1991) ignored pick-up O^+ ions. The simulations used high spatial resolution especially within the magnetic barrier region. If such a model simulated properly all the actual features of the solar wind interaction with Venus including the magnetic field asymmetry and the bow shock shape obviously no substantial effect from the O^+ ions exists. However Brecht and Ferrante (1991) found the pick-up O^+ ions must contribute substantially to fit the bow shock position as measured by PVO. However, the necessary intensity of O^+ ion production cannot be estimated using this approach.

The hybrid simulation by Moore *et al.* (1991) was performed especially to explore the effects caused by the O^+ pick-up ions. But a number of unrealistic assumptions had to be made because of the complexity of the simultaneous dynamics of the solar wind protons and O^+ ions. In particular the spatial resolution in this model was not as high as in the simulation by Brecht and Ferrante (1991). Unfortunately the direct comparison of magnetic field effects in Brecht and Ferrante (1991) and Moore *et al.* (1991) is impossible. Moore *et al.* (1991) claimed that only mass-loading beyond acceptable values would result in a bow shock position close to the mean value inferred from PVO data. Both the mass-loading and the magnetic field barrier are most intensive within a layer of 300–400 km which adjoins the ionopause (obstacle). Therefore, the problem of proper spatial resolution also exists in the case of mass-loading. The boundary conditions at the obstacle seem to be important as well.

To explain the controversy among the Belotserkovskii *et al.* (1987) and Spreiter and Stahara simulations of a mass-loading effect, Stahara and Spreiter (1992) hypothesized that Belotserkovskii *et al.* (1987) had used some ancillary boundary condition which implies constant entropy along the stagnation streamline and obstacle surface when the flow tangency condition at the obstacle was implemented. The strong mass-loading effect was stated by Stahara and Spreiter to be due to the use of an improper boundary condition at the ionopause in Belotserkovskii *et al.* (1987).

Because there also exists a contradiction between the new GD model of Breus *et al.* (1992) and Stahara and Spreiter (1992), it is instructive to discuss the entropy in the case of non-zero mass-loading and the prospects of

any constraint imposed on the entropy along the stagnation streamline in order to implement the flow tangency condition. Moreover, the actual procedure used by Breus *et al.* (1992) for numerical implementation of the flow tangency condition must be examined and this is discussed in Section 2.

The assumptions of the hybrid model of Moore *et al.* (1991), as well as that of Brecht and Ferrante (1991) as well as the spatial resolution in the aforementioned simulations, will be revisited in Section 3 to examine capabilities of both models within the magnetic barrier region where the most intensive mass-loading takes place.

The present day status of numerical simulations can be briefly summarized as follows. The GD simulations by Breus *et al.* (1992) and Stahara and Spreiter (1992) employ the same values of physical parameters of the model. The difference is in the numerical procedure of the implementation of the flow tangency condition. In Breus *et al.* (1992) the 10% effect in shock distance is simulated for the expected photoionization rate. In Stahara and Spreiter (1992) the shock displacement of such an order can occur if the net ionization rate is 5 times that of the expected photoionization. The idea by Zhang *et al.* (1993) that the electron impact ionization significantly exceeds the photoionization is based on over-optimistic estimates. This is unlikely at Venus under the solar activity maximum conditions (see for details Krymskii and Breus (1993)).

The spatial resolution in Moore *et al.* (1991) is insufficient to properly simulate the narrow magnetic barrier region. In Moore *et al.* (1991) the magnetic barrier is broader than in Brecht and Ferrante (1991) and also observed by PVO (Zhang *et al.*, 1991). The cell size in Moore *et al.* (1991) is larger than the magnetic barrier thickness estimated by Zwan and Wolf (1976) and is comparable with the scale height of the neutral oxygen corona.

According to estimates based on the results of Moore *et al.*, the electron impact ionization is less intense than the expected photoionization (Krymskii and Breus, 1993). Thus the physical reason for effective enhancement of the net ion production rate in Moore *et al.* (1991) is unclear. The Brecht and Ferrante (1991) simulation did not specify the ionization intensity which can fit the simulation shock with the shock as measured by PVO.

Further extensive numerical simulations are necessary to estimate accurately the input of different ionization processes and the role of the magnetic barrier in the solar wind interaction with Venus.

2. The generalized entropy balance accounting for new particle creation and numerical implementation of the flow tangency condition

In this section it will be shown that there is a principal reason which makes the entropy per particle inappropriate as one of the GD variables. This reason is that one essentially obtains a two-fluid equation for the entropy per particle if solar protons and O^+ ions form the plasma population. Neither Breus *et al.* (1992) nor Belotserkovskii *et al.* (1987) employed the entropy per particle anywhere in their numerical simulations of the solar wind interaction with Venus. The entropy per particle is usually treated as an intensive thermodynamic variable (Balescy, 1975). This is suitable for the thermodynamics of systems without creation or losses of particles. In principle the entropy per particle can reduce the number of differential equations to be numerically solved in order to simulate the solar wind interaction with a planet disregarding mass-loading. Indeed the set of GD equations can be written as follows:

$$\frac{\partial \rho}{\partial t} + \operatorname{div}(\rho \mathbf{w}) = 0 \tag{1}$$

$$\frac{\partial}{\partial t}(\rho \mathbf{w}) + \rho(\mathbf{w}\cdot\nabla)\mathbf{w} + \mathbf{w}\operatorname{div}(\rho\mathbf{w}) + \nabla p = 0 \tag{2}$$

$$\frac{\partial s}{\partial t} + (\mathbf{w}\nabla)s = 0 \tag{3}$$

$$s = s_1 + c_v \ln \frac{p\rho_1^{\gamma}}{\rho^{\gamma} p_1} \tag{4}$$

(ρ is the mass density of plasma, $\mathbf{w}$ the bulk velocity, p the thermal pressure, s the entropy per particle). The subscript "1" denotes the values on a streamline after shock crossing, $c_v = 3/2$ is the specific heat at constant volume, $\gamma = 5/3$ is the specific heats ratio. Obviously then

$$\frac{p}{\rho^{\gamma}} = \frac{p_1}{\rho_1^{\gamma}} \tag{5}$$

along a streamline is a solution of equation (3). Thus only two differential equations (1) and (2) have to be numerically solved.

Using this approach the boundary condition for the entropy per particle at the impenetrable obstacle is constant, s_1, evaluated at the stagnation line.

The combined equations (1)–(4) presented above are identical to equation (7) in Spreiter *et al.* (1970) if one sets $\partial/\partial t = 0$ and includes the magnetic field $\mathbf{B}$.

As soon as sources or sinks of particles are included, the situation changes. The one-fluid GD relation for the entropy per particle is no longer valid. In general kinetics must be used to investigate the entropy balance of a plasma. The kinetic equation for the distribution function of a plasma component is from Krall and Trivelpiece (1973)

$$\frac{\partial f}{\partial t} + (\mathbf{v}\nabla)f + \frac{Ze}{M}\left(\mathbf{E} + \frac{1}{c}[\mathbf{v}\times\mathbf{B}]\right)\frac{\partial f}{\partial \mathbf{v}} = I(\mathbf{r},\mathbf{v}) + Q(f,\mathbf{v}) \tag{6}$$

where $\mathbf{E}$ and $\mathbf{B}$ are the electric and magnetic field, respectively, Ze the electric charge of a particle, M the mass, I describes the net effect of particle creation and losses, and $Q(f,\mathbf{v})$ the collisional term which does not change the number of particles. Thus the right-hand side of the standard kinetic equation is modified by the term I. The entropy per particle for the plasma component s is then governed by the relation (Balescy, 1975)

$$ns = -\int f \ln f \, \mathrm{d}^3 v + n(1 + \ln(n_0 c_0)) \tag{7}$$

where n is the number density of the component. The last term on the right-hand side of equation (7) ensures that s is dimensionless, with n_0 and c_0 being dimensional constants. From equations (6) and (7) we obtained for the entropy balance

$$\begin{aligned} \frac{\partial}{\partial t}(ns) + \operatorname{div}(ns\mathbf{w}) &= \operatorname{div}\left(nc \int (\mathbf{v}-\mathbf{w}) \hat{f} \ln \hat{f} \, \mathrm{d}^3 v\right) \\ &\quad - \int (1 + \ln f) Q(f, \mathbf{v}) \, \mathrm{d}^3 v \\ &\quad - \int I(\mathbf{r}, \mathbf{v}) \ln \frac{f}{n_0 c_0} \, \mathrm{d}^3 v \\ \mathbf{w} &= c \int \mathbf{v} \hat{f} \, \mathrm{d}^3 v \\ \hat{f} &= \frac{f}{nc} \end{aligned} \tag{8}$$

where the continuity equation

$$\frac{\partial n}{\partial t} + \operatorname{div}(n\mathbf{w}) = \int I(\mathbf{r}, \mathbf{v}) \, \mathrm{d}^3 v \tag{9}$$

has been used to derive equation (8).

It is instructive to compare equation (8) with equations (3) and (4). From equations (1) and (3) one obtains

$$\begin{aligned} \frac{\partial}{\partial t}(\rho s) + \operatorname{div}(\rho \mathbf{w} s) &= 0 \\ \rho &= Mn \end{aligned}$$

which is similar to the left-hand side of equation (8). Obviously two physical factors disturb the standard GD balance of entropy: the non-Maxwellian distribution and the particle creation (losses). The form of equation (7) which is more suitable for the comparison is

$$s = -c \int \hat{f} \ln \hat{f} \, \mathrm{d}^3 v + 1 - \ln \frac{nc}{n_0 c_0}. \tag{10}$$

If the distribution function is assumed to be close to Maxwellian

$$\hat{f} = \exp\left\{-\frac{(\mathbf{v}-\mathbf{w})^2}{v_T^2}\right\} \quad c = (\pi v_T^2)^{-3/2}$$

then equation (10) becomes

$$\begin{aligned} s &= \tfrac{5}{2} + \tfrac{3}{2} \ln \frac{p n_0^{\gamma}}{n^{\gamma} p_0} \\ \gamma &= \tfrac{5}{3}, \quad p = M n v_T^2. \end{aligned} \tag{11}$$

Except for different constants it is similar to equation (4). With the same distribution function the entropy balance equation (8) is

$$\frac{\partial}{\partial t}(ns) + \operatorname{div}(ns\mathbf{w}) = \tfrac{3}{2} \ln \frac{p n_0^{\gamma}}{n^{\gamma} p_0} \int I(\mathbf{r}, \mathbf{v}) \, \mathrm{d}^3 v + \int \frac{(\mathbf{v}-\mathbf{w})^2}{v_T^2} I(\mathbf{r}, \mathbf{v}) \, \mathrm{d}^3 v. \tag{12}$$

This relation is a generalized equation for entropy balance which must be satisfied in any GD model for the solar wind interaction with a planet including a model with non-zero mass loading. The parameters n_0 and p_0 make the right-hand side of equation (12) positive and ensure that the entropy grows with time. The set of GD equations employed in Breus *et al.* (1992) and earlier in Belotserkovskii *et al.* (1987) does not contradict this generalized entropy balance equation. In those publications $I(\mathbf{r}, \mathbf{v}) = I(\mathbf{r})\delta(\mathbf{v})$ was required for new-born O^+ ions. The following multi-species system of GD equations can be derived directly from the kinetic equations for the protons and O^+ ions assuming the Maxwell distribution for each species

$$\frac{\partial}{\partial t} n_p + \operatorname{div}(n_p \mathbf{w}_p) = 0 \tag{13}$$

$$\frac{\partial}{\partial t} n_i + \operatorname{div}(n_i \mathbf{w}_i) = I(\mathbf{r}) \tag{14}$$

$$M_p \left\{\frac{\partial}{\partial t}(n_p \mathbf{w}_p) + \operatorname{div}(n_p \mathbf{w}_p : \mathbf{w}_p)\right\} + \nabla p_p = -\mathbf{R}_{ip} \tag{15}$$

$$M_p \mu \left\{\frac{\partial}{\partial t}(n_i \mathbf{w}_i) + \operatorname{div}(n_i \mathbf{w}_i : \mathbf{w}_i)\right\} + \nabla p_i = \mathbf{R}_{ip} \tag{16}$$

$$\frac{\partial}{\partial t}\left(M_p n_p \frac{w_p^2}{2} + \tfrac{3}{2} p_p\right) + \operatorname{div}\left\{\mathbf{w}_p\left(M_p n_p \frac{w_p^2}{2} + \tfrac{5}{2} p_p\right)\right\} = -Q_{ip} \tag{17}$$

$$\frac{\partial}{\partial t}\left(\mu M_p n_i \frac{w_i^2}{2} + \tfrac{3}{2} p_i\right) + \operatorname{div}\left\{\mathbf{w}_i\left(\mu M_p n_i \frac{w_i^2}{2} + \tfrac{5}{2} p_i\right)\right\} = Q_{ip} \tag{18}$$

where $\mathbf{R}_{ip}$ is the generalized drag force between O^+ ions and the solar protons, while Q_{ip} is the energy exchange rate, and μ the atomic weight (a.m.u.).

For the numerical simulation we take the following set of equations:

$$\frac{\partial}{\partial t} n_p + \operatorname{div}(n_p \mathbf{w}) = 0 \tag{19}$$

$$\frac{\partial}{\partial t} n_i + \operatorname{div}(n_i \mathbf{w}) = I(\mathbf{r}) \tag{20}$$

$$\frac{\partial}{\partial t}[(n_p + \mu n_i)\mathbf{w}] + \operatorname{div}[(n_p + \mu n_i)\mathbf{w} : \mathbf{w}] + \frac{1}{M_p} \nabla p = 0 \tag{21}$$

$$\frac{\partial}{\partial t}\left[M_p(n_p+\mu n_i)\frac{w^2}{2}+\tfrac{3}{2}p\right]$$

$$+\operatorname{div}\left\{\mathbf{w}\left[M_p(n_p+\mu n_i)\frac{w^2}{2}+\tfrac{5}{2}p\right]\right\}=0$$

$$p=p_e+p_i \tag{22}$$

which was derived by Breus *et al.* (1992) from equations (13) and (14). The difference in bulk velocities of protons and O^- ions is neglected in comparison with the common bulk velocity of plasma **w**. As is clear from equations (19) to (22) the bulk velocity of the flow is more sensitive to the combinations $n_p+\mu n_i$, p_p+p_i, than to the individual value of each physical variable therein. There is no restriction imposed on the ratio p_i/p_p. Further assumptions are necessary to replace equation (22) by the equation of entropy balance of the one-fluid type. Only equal temperatures of plasma components and constant ratio n_i/n_p throughout the magnetosheath permit a one-fluid type entropy equation.

Indeed the entropy per particle for a two ion system of protons and O^+ ions is

$$s=\frac{(n_p s_p+n_i s_i)}{(n_p+n_i)} \tag{23}$$

or

$$s=s_p+\frac{n_i}{n_p+n_i}(s_i-s_p)=s_p$$

$$-\frac{n_i}{n_p+n_i}\tfrac{3}{2}\ln\left[\frac{p_p}{p_{p0}}\frac{p_{i0}}{p_i}\left(\frac{n_i}{n_{i0}}\right)^{\gamma}\left(\frac{n_{p0}}{n_p}\right)^{\gamma}\right]. \tag{24}$$

The one-fluid GD model gives the following value for the entropy per particle:

$$s=\tfrac{5}{2}+\tfrac{3}{2}\ln\left[\frac{p}{(n_p+n_i)^{\gamma}}\frac{(n_{p0}+n_{i0})^{\gamma}}{p_0}\right].$$

The right-hand side of this equation can be identical to the right-hand side of equation (11) only if the conditions mentioned above are satisfied. The equation which describes the evolution of the entropy along the streamline can be deduced from equation (24). It is

$$\frac{ds}{dt}=-\frac{3}{2}\frac{d}{dt}\left\{\frac{n_i}{n_p+n_i}\ln\left[\frac{p_p}{p_{p0}}\frac{p_{i0}}{p_i}\left(\frac{n_i}{n_{i0}}\right)^{\gamma}\left(\frac{n_{p0}}{n_p}\right)^{\gamma}\right]\right\}. \tag{25}$$

The conservation of the proton entropy $ds_p/dt=0$ was employed to get equation (25). The conservation of proton entropy is straightforward from equations (12) and (19).

The right-hand side of equation (25) is dependent on the characteristics of both ion populations in the plasma and is unsuitable for any one-fluid GD simulation. Therefore, the entropy per particle was not employed at any stage and in any form in simulations by Breus *et al.* (1992) or Belotserkovskii *et al.* (1987). In the two-fluid model by Breus *et al.* (1992) the total plasma pressure p and the plasma mass density $n_p+\mu n_i$ should satisfy

$$\frac{d}{dt}\ln\left[\frac{p}{(n_p+\mu n_i)^{\gamma}}\right]=$$

$$-\frac{5}{3}\left[1-\frac{2M_p(n_p+\mu n_i)w^2}{5p}\right]\frac{\mu I}{(n_p+\mu n_i)} \tag{26}$$

which follows from equations (19) to (22). The left-hand side of this equation can be written as ds/dt if the one-fluid relation for the entropy per particle is assumed to be valid. This is physically incorrect in the case of non-zero mass-loading within the magnetosheath at Venus. Nevertheless Stahara and Spreiter (1992) used the values of $p/(n_p+\mu n_i)^{\gamma}$ along the streamline to examine the entropy per particle along the stagnation line in Belotserkovskii *et al.* (1987). In spite of this misinterpretation the variations of $p/(n_p+\mu n_i)^{\gamma}$ are useful for comparison of Stahara *et al.*'s (1987) and Breus *et al.*'s (1992) results but it is unable to explain the difference between the simulations.

As one can see from Table 1 the simulations differ from each other most prominently in the vicinity of the impenetrable obstacle. The mass density in Breus *et al.* (1992) is intermediate to the simulation with zero mass-loading and the results by Stahara and Spreiter (1992) obtained for the expected photoionization of the oxygen corona. The thermal pressure in Breus *et al.* (1992) is minimal. There is a very high gradient in the mass density and consequently in $p/(n_p+\mu n_i)^{\gamma}$ as simulated by Stahara and Spreiter (1992). In contrast the mass density at the impenetrable obstacle in Breus *et al.* (1992) is lower by a factor of 2 and an insignificant decrease in $p/(n_p+\mu n_i)^{\gamma}$ toward the obstacle was simulated. It follows from equation (26) that in close proximity of the stagnation point we have

$$\frac{d}{dt}\ln\frac{p}{(n_p+\mu n_i)^{\gamma}}=-\frac{5}{3}\frac{\mu I}{(n_p+\mu n_i)}. \tag{27}$$

Obviously the high density in Stahara and Spreiter (1992) implies a lower right-hand side and lower effects of mass-loading itself in variations of $p/(n_p+\mu n_i)^{\gamma}$ along the stagnation streamline. This conclusion is in contrast with the simulation results displayed in Fig. 1. Therefore, the difference of the simulation results is not a consequence of the non-zero mass-loading itself but of a difference in the numerical codes.

In Breus *et al.* the flow tangency condition was implemented via a reflection procedure. According to this procedure a row of ghost computational points is added at the edge of the computational domain which is half of a dayside magnetosheath transformed in a rectangle according to the law given in the Appendix.

The ghost points are located at the same normal distance to the boundary of the physical domain as the corresponding mesh points within the edge rows of the physical domain. The details of the reflection procedure itself are given in the Appendix.

In Stahara and Spreiter's model the mesh points are located at the impenetrable obstacle surface. In principle this method can be more sensitive to the unlimited derivatives of the mass density in the vicinity of the obstacle. The special procedure had been employed in Stahara and Spreiter to make the code second-order accurate at the

Table 1. Results

Models	Stahara and Spreiter (1987, 1991)	Belotserkovskii *et al.* (1987), Breus *et al.* (1992)	Brecht and Ferrante (1991) N2	Brecht and Ferrante (1991) N6	Moore *et al.* (1991) (1992)
Effect on the BS position	No mass-loading effect for I_∞	Substantial mass-loading effect for I_∞	Magnetic barrier does not deflect the solar wind effectively. Substantial mass-loading necessary to fit BS with observed position. Fine resolution is necessary		No mass-loading effect. Very strong effect of magnetic barrier on BS position
Reason disagreements	Strong effect of mass-loading by Belotserkovskii *et al.* and Breus [3] is an artifact resulting from boundary conditions: constant entropy along stagnation and wetting streamlines	The entropy per particle was not used as one of the GD variables either by Belotserkovskii *et al.* or by Breus *et al.*, as well as an ancillary condition employed when the flow tangency condition at the ionopause surface was implemented	Agreement exists with Breus *et al.* (1992) in the estimation of mass-loading effect. The fine resolution is necessary and strong input of computational process itself on the magnetic field is expected. Asymmetry of magnetic field much in excess of mean PVO values		Very strong effect on the magnetic barrier is expected because of the spatial resolution was poor in both simulations as mentioned by Brecht and Ferrante. Minimal thickness of cell 100 km is only half of the neutral scale height of 200 km used in model

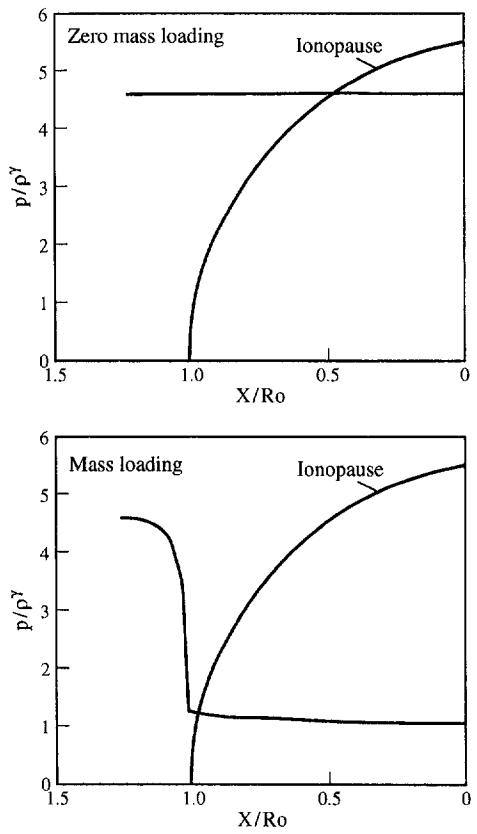

Fig. 1. Ratio p/ρ^γ along stagnation streamline for zero and non-zero mass-loading (Stahara and Spreiter, private communication).

boundary. At the boundary additional points in the normal direction in the differencing stencil were employed to insure that the discretized finite difference equations retain second-order spatial accuracy at those locations.

The ambiguity of the flow tangency condition in GD simulation with/without mass-loading which can lead to the uniqueness of the solution have been already discussed in Breus *et al.* (1992). Here we continue to discuss this problem.

The theorem by Coshi-Kovalevskaya can provide a proof of the uniqueness of GD solutions. Under axial symmetry the steady state solution is dependent on only two spatial variables and Coshi-Kovalevskaya's theorem can be straightforwardly applied. As one can conclude, the conditions imposed by this theorem may be unsatisfied in the case of non-zero mass-loading. In particular this theorem implies the equation of state is an analytical function, that is its partial derivatives are coupled to each other.

Thus, if there are some singular points the uniqueness is questioned. As well the singular points must have an impact on the discretization and on the numerical solution. This can be very critical for the numerical implementation of the boundary conditions if there are any singular points at the boundary.

Therefore, the analysis of the approximate solution of the GD equations in partial derivatives which is valid in the vicinity of the stagnation point can cast new light on the uniqueness of the solution to the GD equations and on the numerical implementation of the flow tangency condition.

Let us begin with the equation for total plasma pressure, equation (26).

This equation is the state equation in the case of non-zero mass-loading. Under the steady state conditions equation (26) takes the form

$$(\mathbf{w}\nabla)\ln\frac{p}{(n_p+\mu n_i)^{\gamma}} = -\frac{5}{3}\left(1-\frac{2M_p(n_p+\mu n_i)w^2}{5p}\right)\cdot\frac{\mu I}{(n_p+\mu n_i)}. \quad (28)$$

At the stagnation streamline which comes to the stagnation point the tangential velocity w_t must be zero due to axial symmetry. As a consequence equation (28) can be written in the form

$$w_n\frac{\partial}{\partial\xi}\ln\frac{p}{(n_p+\mu n_i)^{\gamma}} = \frac{5}{3}\left(1-\frac{2M_p(n_p+\mu n_i)w_n^2}{5p}\right)\cdot\frac{\mu I}{(n_p+\mu n_i)} \quad (29)$$

where the coordinate ξ is the distance from the obstacle along the stagnation streamline. Note that the stagnation streamline is along the normal to the impenetrable obstacle therein.

In the proximity of the obstacle $w_n = 0$ and the following Taylor series

$$w_n = \left.\frac{\partial w_n}{\partial\xi}\right|_{\xi=0}\xi$$

is a reasonable approximation.

Because of physical constraints the gradients of the plasma pressure within the nose region are small enough and it follows from equation (3) that the mass density of plasma $n_p+\mu n_i$ obeys an equation

$$\left.\frac{\partial w_n}{\partial\xi}\right|_{\xi=0}\xi\cdot\frac{\partial}{\partial\xi}(n_p+\mu n_i) = -\mu I.$$

The local approximate solution is straightforward

$$n_p+\mu n_i = A_0+\mathscr{A}_1\ln\frac{\xi}{\xi_0}$$

where $\mathscr{A}_1 < 0$ to make $n_p+\mu n_i$ positive in the stagnation point $\xi = 0$. For $\mathscr{A}_1$ one has

$$\mathscr{A}_1 = -\mu I\left.\frac{\partial w_n}{\partial\xi}\right|_{\xi=0}^{-1}. \quad (30)$$

The flow stagnates at the obstacle and $\partial w_n/\partial\xi|_{\xi=0} > 0$. Thus the solution given here is physically reasonable.

It is easy to see $\mathscr{A}_1 = 0$, if $I = 0$ that the solution has no peculiarity at $\xi = 0$. In other words the stagnation point is not peculiar for the solution of the GD equations in partial derivatives. In contrast $n_p+\mu n_i$ is unlimited if $I \neq 0$ and $\xi = 0$.

Therefore, the stagnation point becomes peculiar as soon as $I \neq 0$. The solution presented here nevertheless satisfies the flow tangency condition

$$w_n(n_p+\mu n_i) \sim \xi\cdot\ln\frac{\xi}{\xi_0} \to 0 \quad \text{when } \xi \to 0.$$

If this solution is extended in the region surrounding the stagnation point then

$$n_p+\mu n_i = \mathscr{A}_0(\xi,\theta)+\mathscr{A}_1(\xi)\ln\frac{w_n(\xi,\theta)}{w_0}$$

where ξ and θ are the coordinates along the normal and the tangential coordinates, respectively, w_0 is a dimensional constant.

The function $\mathscr{A}(\xi)$ satisfies the condition

$$\mathscr{A}_1(\xi) < 0$$

and

$$\mathscr{A}_1\left(\frac{\mathbf{w}}{w_n}\nabla\right)w_n = \mu I. \quad (31)$$

Obviously it presumes that

$$\left(\frac{\mathbf{w}}{w_n}\nabla\right)w_n < 0.$$

That is w_n increases outward, $\mathbf{w} = -w_n\mathbf{e}_n+w_e\mathbf{e}_e$. The terms like

$$w_n\ln\frac{w_n}{w_0}\cdot\frac{dA_1}{d\xi}$$

and

$$(\mathbf{w}\nabla)A_0$$

were neglected due to $w_n = 0$ if $\xi = 0$ to get equation (31).

The flow tangency condition is also satisfied:

$$w_n(n_p+\mu n_i) = 0 \quad \text{if } \xi = 0.$$

Such unlimited plasma density $n_p+\mu n_i$ and unlimited derivatives mean there is a peculiarity in the subsolar point and perhaps at the obstacle surface. Consequently the equation of state is no longer analytical and the uniqueness of the solution for the GD equations in partial derivatives should be specially proven.

The numerical computations cannot be done with arbitrary spatial resolution and with unlimited values. Therefore, there is a regularization when the equations are discretized. The regularization depends on the numerical scheme employed in the simulation.

Regardless of this the physical sense of the unlimited mass density is a matter of discussion. In reality the mass density is limited everywhere and the peculiarity in the stagnation point is a consequence of simplifications done to come to the GD model. Thus the regularization is required to be physically reasonable.

It is a paradox that the more accurately the numerical solution reproduces the GD solution in the vicinity of the stagnation point the further it can be from reality. And no one criterion which is to select physically reasonable regularization can be obtained employing the gas-dynamics and computational mathematics.

As one can see from the results presented by Breus *et al.* and Stahara and Spreiter the mass density within the stagnation point is finite in both models. Thus none of them reproduced accurately the solution of the GD equations within this point. But the higher mass density and sharper

gradients in Stahara and Spreiter are closer to the solution of the GD equations in partial derivatives. Nevertheless the question of which numerical model is in better agreement with observations is a matter for discussion.

Finally we can discuss the plasma depletion within the interplanetary magnetic field (IMF) build-up region as a proxy for the physical process which makes the plasma density finite throughout the dayside magnetosheath.

The GD model corresponds to the $M_A \to \infty$ limit of the more general MHD model. As one can see from the analysis presented above, the physically unreal growth of the plasma density occurs at the impenetrable obstacle where the non-zero IMF effects can no longer be ignored even if M_A is high enough.

There are two more general approaches which allow us to analyse the effect of the non-zero IMF. One is the hybrid model and another one is the MHD model already mentioned. Let us discuss briefly the results obtained within the framework of the approaches which are available today.

It was found in the hybrid simulation of the solar wind interaction with Venus which was done by Moore *et al.* (1991) that the plasma density is about zero in the close proximity of the obstacle. Perhaps this is an effect of the absorbing obstacle and the plasma density is non-zero in reality, but nevertheless the infinite density was not simulated and obviously the density was much less than that in Stahara and Spreiter's paper.

Recently McGary and Pontius (1994) have attempted to analyse the IMF build-up effect. Unfortunately they ignored the plasma depletion along the magnetic field lines because of two-dimensional geometry which they presumed to make the calculation possible. The physically unrealistic solution for the plasma density having a singularity at the obstacle is also valid in their model.

At the same time the reflection procedure used by Breus *et al.* for implementation of the flow tangency condition seems to suit better a boundary layer where the IMF effect (a plasma depletion) is important, since it ignores any singularity which is beyond the GD flow region.

This is likely the reason for the disagreement between the Stahara and Spreiter and Breus *et al.* models.

3. Comparative analysis of principal parameters and results of hybrid models of solar wind interaction with Venus

The standard set of kinetic equations for protons and O^+ ions can be used to specify parameters of hybrid simulations by Moore *et al.* (1991) and Brecht and Ferrante (1991). The values ascribed to the model in order to make simulations run possible should be compared with values expected at Venus. Consequently the reliability of simulation results can be better understood. The set of equations which describe the dynamics of protons and O^+ ions is

$$\frac{\partial f_i}{\partial t} + (\mathbf{v}\nabla) f_i - \frac{\Omega_p}{\mu}(\mathbf{w}-\mathbf{v}) \times \mathbf{B}/B \frac{\partial f_i}{\partial \mathbf{v}} + \frac{e}{\mu M_p} \mathbf{E}_h \frac{\partial f_i}{\partial \mathbf{v}} = I(\mathbf{r})\delta(\mathbf{v}) \quad (32)$$

$$\frac{\partial f_p}{\partial t} + (\mathbf{v}\nabla) f_p - \Omega_p(\mathbf{w}-\mathbf{v}) \times \mathbf{B}/B \frac{\partial f_p}{\partial \mathbf{v}} + \frac{e}{M_p} \mathbf{E}_h \frac{\partial f_p}{\partial \mathbf{v}} = 0 \quad (33)$$

the magnetic field $\mathbf{B}$

$$\frac{1}{c}\frac{\partial \mathbf{B}}{\partial t} = -\nabla \times \mathbf{E} \quad (34)$$

the electric field $\mathbf{E}$

$$\mathbf{E} = -\frac{1}{c}[\mathbf{w}, \mathbf{B}] + \mathbf{E}_h \quad (35)$$

$$\mathbf{E}_h = \frac{1}{en}\left(-\nabla p_e + \frac{1}{4\pi}(\nabla \times \mathbf{B}) \times \mathbf{B}\right) \quad (36)$$

and electrons

$$n = \int (f_p + f_i)\, \mathrm{d}^3 v \quad (37)$$

$$\mathbf{w} = \frac{1}{n}\int \mathbf{v}(f_p + f_i)\, \mathrm{d}^3 v \quad (38)$$

$$\frac{\partial n}{\partial t} + \mathrm{div}\,(n\mathbf{w}) = I. \quad (39)$$

Obviously the number of equations (32)–(39) is larger than the number of variables to be specified. The electron temperature of the plasma may be treated as an external parameter of the model. The continuity equation for the plasma electrons imposes an additional restriction on the proton and ion flow

$$\frac{\partial n}{\partial t} + \mathrm{div}\left(\int \mathbf{v}(f_p + f_i)\, \mathrm{d}^3 v\right) = I. \quad (40)$$

Thus not all the components of ion fluxes are actually independent. The continuity equation (36) is unemployed by all hybrid models. Each component of each ion flux is computed independently. The numerical errors in fluxes along the maximum variation direction can produce critical variations in simulation results. Before the computational run becomes possible the equations should be written for dimensionless variables. To compare the model with the actual solar wind interaction with Venus the following dimensionless parameters are convenient:

$$\tau = \frac{t u_0}{R_0}, \quad \hat{\mathbf{w}} = \frac{\mathbf{w}}{u_0}, \quad \hat{\mathbf{v}} = \frac{\mathbf{v}}{u_0}, \quad \hat{\mathbf{B}} = \frac{\mathbf{B}}{u_0},$$

$$\hat{n} = \frac{n}{n_0}, \quad \hat{f}_p = \frac{f_p u_0^3}{n_0}, \quad \hat{f}_i = \frac{f_i u_0^3}{n_0} \quad (41)$$

where n_0 and u_0 are the number density and bulk velocity of ambient solar wind, B_0 the strength of unperturbed IMF. The planetary radius R_0 should be a unity of spatial grid. Under these assumptions the following dimensionless equations which describe the ions should be solved numerically:

$$\frac{\partial \hat{f}_i}{\partial \tau} + (\hat{\mathbf{v}}\nabla)\hat{f}_i - \frac{\Omega'_p R_0}{\mu u_0}[(\hat{\mathbf{w}} - \hat{\mathbf{v}}) \times \hat{\mathbf{B}}]\frac{\partial \hat{f}_i}{\partial \hat{\mathbf{v}}} + \frac{1}{\mu}\hat{\mathbf{E}}_h \frac{\partial \hat{f}_i}{\partial \hat{\mathbf{v}}} = \frac{IR_0}{n_0 u_0}\delta(\hat{\mathbf{v}}) \quad (42)$$

$$\frac{\partial \hat{f}_p}{\partial \tau} + (\hat{\mathbf{v}}\nabla)\hat{f}_p - \frac{\Omega'_p R_0}{u_0}[(\hat{\mathbf{w}} - \hat{\mathbf{v}}) \times \hat{\mathbf{B}}]\frac{\partial \hat{f}_p}{\partial \hat{\mathbf{v}}} + \hat{\mathbf{E}}_h \frac{\partial \hat{f}_p}{\partial \hat{\mathbf{v}}} = 0 \quad (43)$$

$$-\frac{\partial \hat{\mathbf{B}}}{\partial \tau} = \nabla \times \hat{\mathbf{E}} \quad (44)$$

$$\hat{\mathbf{E}} = -\hat{\mathbf{w}} \times \mathbf{B} + \frac{u_0}{\Omega'_p R_0}\hat{\mathbf{E}}_h \quad (45)$$

$$\hat{\mathbf{E}}_h = \frac{1}{\hat{n}}\left\{-\nabla p_e + \frac{1}{M_A^2}(\nabla \times \hat{\mathbf{B}}) \times \hat{\mathbf{B}}\right\}. \quad (46)$$

To carry out an adequate simulation of the real situation the actual values of the ratio $\Omega'_p R_0/u_0$, $I(R/R_0) \cdot R_0/n_0 u_0$ and the atomic weight of planetary ions, as well as the Alfvenic Mach number of ambient solar wind have to be prescribed to the model. When the planetary ion effects are ignored as in Brecht and Ferrante (1991), only two parameters are characteristic to the numerical simulation: namely $\Omega'_p R_0/u_0$ and M_A.

Brecht and Ferrante (1991) concentrated on the magnetic field effects. A number of simulations were made to study the effect of computational cell size on the subsolar bow shock position and the subsolar magnetic barrier structure. The subsolar region of a planet with 6000 km radius was simulated twice. One simulation has crude resolution: 100 km in the sunward direction and 360 km in the other direction (simulation No. 3 therein) and another one is of much finer resolution: 40–50 km in the sunward direction and 100 km in others (simulation No. 6). One finds that fine resolution is in fact necessary for a proper simulation. Thus the resolution in the sunward direction should be better than 6.7×10^{-3} R_0 (R_0 is the planetary radius prescribed to the model) and 1.7×10^{-2} R_0 in other directions. Moore *et al.*'s (1991) simulations concentrated on the effects of O^+ pick-up ions. Because of the computational constraints a reduced atomic weight of O^+ ion $\mu = \mu_0/2$ and the reduced radius of planet $R_0 = R_v/2$ ($\mu = 16$ a.m.u. is the actual weight of O^- ion, R_v is the radius of Venus) were used in the model. Under these circumstances the ratio of the planetary radius to the gyroradius of O^+ ions

$$\frac{\Omega'_p R_0}{\mu u_0} = \frac{\Omega'_p R_v}{\mu_0 u_0}$$

retains its actual value. The right-hand side of equation (42) takes the same value as at Venus if $I = 2I_v$ (I_v is the actual rate of O^+ ion formation at Venus) is prescribed to the model. The last term on the left-hand side of equation (42) describes the Hall electric field effect on O^- ions. It is twice the actual value and a stronger depletion of O^+ ions within the magnetic barrier region is expected. In equation (43) the ratio of the planetary radius to the proton gyroradius is only half of the value expected at Venus

$$\frac{\Omega'_p R_0}{u_0} = \frac{\Omega'_p R_v}{2u_0}.$$

As a result the finite gyroradius effect of the solar protons is two times stronger compared with the parameters of Venus.

It was already mentioned that the O^+ ion formation rate $I = 2I_v$ provides the actual value of the O^+ ion abundance. But only a number density of O^+ ions twice as high as its actual value can generate a drag force due to O^+ ion pick-up comparable with the Hall electric field and can give a proper value to the mass-loading effect. Indeed the total electric field $\mathbf{E}$ can be presented as

$$\hat{\mathbf{E}} = -[\hat{\mathbf{u}}_p \times \hat{\mathbf{B}}] + \frac{\hat{n}_i}{\hat{n}}[(\hat{\mathbf{u}}_p - \hat{\mathbf{u}}_i) \times \hat{\mathbf{B}}] + \frac{2u_0}{\Omega'_p R_v}\frac{1}{\hat{n}}\left[-\nabla \hat{p}_e + \frac{1}{M_A^2}[(\nabla \times \hat{\mathbf{B}}) \times \hat{\mathbf{B}}\right]$$

$$\hat{\mathbf{u}}_p = \int \frac{\mathbf{v} f_p \, d^3v}{u_0} \Big/ \int f_p \, d^3v$$

$$\hat{\mathbf{u}}_i = \int \frac{\mathbf{v} f_i \, d^3v}{u_0} \Big/ \int f_i \, d^3v. \quad (47)$$

The second term on the right-hand side of equation (47) is proportional to the difference of bulk velocities of solar protons and O^+ ions and describes the deceleration of the protons due to the pick-up of O^+ ions. The third term contains the Hall electric field resulting from the magnetic field build-up within the magnetic barrier. An even more intense ionization rate: $I = 4I_u$ should be used in the model to move the mass-loading effect close to its actual value at Venus. If it is so the mass density of plasma and the mass production rate become close to the value expected for the GD models by Breus *et al.* (1992) and Stahara and Spreiter (1992). Indeed one obtains the continuity equation

$$\operatorname{div}\left(\hat{n}_p \hat{\mathbf{u}}_p + \frac{\mu_0}{2}\hat{n}_i \hat{\mathbf{u}}_i\right) = \frac{I\mu_0 R_v}{4u_0 n_0}$$

after the integration of the sum of equations (42) and (43). Obviously the O^+ ions should be two times more abundant and the ionization rate should be increased by a factor of 4 to fit the hybrid model by Moore *et al.* (1991) with the GD models with non-zero mass-loading.

Initially numerical simulation with cells of $102 \times 360 \times 360$ km^3 size and the planet of 3000 km radius was done by Moore *et al.* (1991). Such cells look unsuitable for the proper simulation of the magnetic barrier region and mass loading at Venus. Indeed the subsolar magnetic barrier thickness was estimated from the *in situ* PVO data as 200 km (Zhang *et al.*, 1991). As well the analytical MHD treatment of the magnetic barrier region by Zwan and Wolf (1976) gave a magnetic barrier size of R_0/M_A^2 (R_0 is the curvature radius of the obstacle). If the typical M_A at Venus is presumed the Zwan and Wolf (1976) estimate is very close to the value estimated from *in situ* data. Since the radius of the planet used in the model is only half of the actual value the magnetic barrier

Table 2. Parameters and results of different simulations parameters

Input parameters	Stahara and Spreiter (1987, 1991) [13, 17]	Belotserkovskii *et al.* (1987) [15]	Breus *et al.* (1992) [16]	Brecht and Ferrante [11] (1991) N2	(1991) N6	Moore *et al.* (1991) [12]	(1992) private communication
Goals of model	GD model mass-loading effect on BS position	GD one-fluid mass-loading effect	GD two-fluid mass-loading effect	Hybrid model magnetic barrier effect		Hybrid model mass-loading effect	
Mach number	$M_{MS} = 5.7$	$M_{MS} = 5.7$	$M_{MS} = 5.7$	$M_{MS} = M_A = 5$	$M_{MS} = M_A = 5$	$M_{MS} = M_A = 5$	
Obstacle radius	$R_0 = R_v$	$R_0 = R_v$	$R_0 = R_v$	$R_0 = R_v$	$R_0 = R_v/2$	$R_0 = R_v/2$	
Mass-loading intensity	$I = I_v$	$I = I_v$	$I = I_v$	$I = 0$	$I = 0$	$I = I_v/2$	$I = 5I_v$
n_i/n_p	$\neq 0$	$\neq 0$	$\neq 0$	$= 0$	$= 0$	$\neq 0$	$\neq 0$
Mass of heavy ion	16	16	16			8	8
λ^*/R_0	0	0	0	$R_0/\rho_p = 8.22$	16.4	8.22	8.22
Size of computational cell in sunward direction				100 km	40–50 km	200 km	100 km
in other direction				360 km	100 km	760 km	360 km

λ^*—free path of proton; ρ_p— proton gyroradius $\rho_p = u_0/\Omega_p'$, $\Omega_p' = eB_0/Mpc$; u_0—ambient solar wind velocity; R_0—Venus radius; I_v—empirical mass-loading source [13].

size should also be half of the actual thickness 200 km, that is, 100 km. Of course this presumes that the model is adequate to the situation at Venus. Obviously the initial simulation by Moore *et al.* (1991) was too crude to resolve magnetic barrier of adequate thickness.

Later Moore *et al.* (1992) performed a new simulation with cells $51 \times 180 \times 180$ km^3 (Moore, private communication). The situation looks better but even in this case there are only two cells for the adequate magnetic barrier thickness. Using the planetary radius scaling one obtains 1.7×10^{-2} R_0 in the sunward direction and 6×10^{-2} R_0 in other directions. If the dimensionless cell size and the parameter $R_0\Omega_p'/u_0$ in Moore *et al.* (1992) are compared with the Brecht and Ferrante (1991) simulation the new run by Moore *et al.* is very close to simulation No. 3 in Brecht and Ferrante when the enormous effect of the magnetic barrier is simulated. The mass-loading effect is disregarded for such comparison. In general the rectangular cells of the hybrid model are more convenient for the simulation of particle dynamics than for a localized boundary layer structure like a magnetic barrier. Namely the magnetic barrier follows the shape of the obstacle and most intensive variations of the parameters therein are along the normal to the obstacle surface. The normal to the obstacle surface is not everywhere in the sunward direction which is of the finest resolution in the hybrid model. Therefore, the effective resolution of the magnetic barrier region becomes more crude at the flanks. Possibly the stronger simulated asymmetry in the magnetic field strength when it is compared with the measured asymmetry is partly due to the decrease in the effective resolution of the magnetic barrier from nose point to flanks.

4. Conclusion

The comparative analysis of the simulations of the solar wind interaction with Venus which are available at present is summarized in Table 2. The substantial effect of the mass addition to the flow (the pick-up ions) on the shock geometry at Venus is confidently established. But the magnitude of the mass addition rate which is able to produce the observed shock geometry is controversial. The difference between Breus *et al.* (1992) and Stahara and Spreiter (1992) is likely a result of different numerical implementation of the flow tangency condition which does not permit the specification of the equation of state $p = p(\rho)$ at the impenetrable obstacle because of its ambiguity.

The abrupt drop of the ratio $p/(n_p + \mu n_i)^\gamma$ in the vicinity of the impenetrable obstacle as reported by Stahara and Spreiter (1992), is unrelated to the non-zero intensity of the mass-loading. It is probably due to the ambiguous equation of state at the obstacle which should be employed for the mesh points there.

The numerical code by Breus *et al.* (1992) uses the reflection procedure for the implementation of the flow tangency condition and is insensitive to the equation of state at the obstacle surface. The magnetic barrier does not deflect the solar wind effectively enough to fit the bow shock position inferred from the hybrid simulations with actual mean bow shock at Venus (Brecht and Ferrante, 1991, simulation No. 6).

The hybrid simulations which account for O^+ ions and allows spatial resolution better than 6.7×10^{-2} R_0 in the sunward direction and 1.7×10^{-2} R_0 in other directions could likely resolve existing controversy. The unusually high effect of the electron impact ionization can fit the results of the simulation by Stahara and Spreiter (1992) with observations.

In contrast Breus *et al.* (1992) simulated the proper geometry of the shock at Venus for the electron impact ionization at a level of 60% of the photoionization rate during the solar activity maximum.

Acknowledgements. The authors thank very much Drs S. Brecht

and K. Moore for the discussion of the hybrid simulation results, and Dr S. Stahara and Professor J. Spreiter who kindly presented high resolution numerical data and figures on the GD simulation of the solar wind interaction with Venus. We are deeply appreciative to Professor J. F. McKenzie for his helpful discussion and valuable comments on GD code problems. The authors thank the Max Planck Society for providing financial support. The research described in this publication was made possible in part by Grant No. N7R000 from the Internation Science Foundation.

References

Balescy, R., *Equilibrium and Nonequilibrium Statistical Mechanics*. Wiley, New York, 1975.

Belotserkovskii, O. M., Breus, T. K., Krymskii, A. M., Mitnitskii, V. Ya., Nagy, A. F. and Gombosi, T. I., The effect of hot oxygen corona on the interaction of Solar Wind with Venus. *Geophys. Res. Lett.* **14,** 503, 1987.

Brecht, S. H. and Ferrante, J. R., Global hybrid simulation of unmagnetized planets: comparison of Venus and Mars. *J. geophys. Res.* **96,** 11209–11220, 1991.

Breus, T. K. and Krymskii, A. M., Turbulent pick-up of new born ions near Venus and Mars and problems of numerical modeling of the solar wind interaction with these planets. 1. Features of the solar wind interaction with planets. *Planet. Space Sci.* **40,** 121–130, 1992.

Breus, T. K., Krymskii, A. M. and Mitnitskii, V. Ya., Turbulent pick-up of new born ions near Venus and Mars and problems of numerical modeling of the solar wind interaction with these planets, 1. Two-fluid GD model. *Planet. Space Sci.* **40,** 131–138, 1992.

Krall, N. A. and Trivelpiece, A. W., *Principles of Plasma Physics*. McGraw-Hill, New York, 1973.

Krymskii, A. M. and Breus, T. K., Comments on the paper "Oxygen ionization rates at Mars and Venus: relative contribution of impact ionization and charge-exchange" by M. H. G. Zhang, J. G. Luhmann, A. F. Nagy, J. R. Spreiter and S. S. Stahara. *J. geophys. Res.* 1993, submitted.

Mihalov, J. D., Spreiter, J. R. and Stahara, S. S., Comparison of gas-dynamic model with solar wind flow around Venus. *J. geophys. Res.* **87,** 10363, 1982.

Moore, K. R., Thomas, V. A. and McComas, D. J., Global hybrid simulation of the solar wind interaction with the dayside of Venus. *J. geophys. Res.* **96,** 7779–7791, 1991.

Roach, P. J., *Computational Fluid Dynamics*. Hermosa, Albuquerque, 1976.

Spreiter, J. R. and Stahara, S. S., A new predictive model for determining solar wind terrestrial planet interactions. *J. geophys. Res.* **85,** 6769, 1980a.

Spreiter, J. R. and Stahara, S. S., Solar wind flow past Venus: theory and comparisons. *J. geophys. Res.* **85,** 7715, 1980b.

Spreiter, J. R., Summers, A. and Alksne, A. Y., Hydromagnetic flow around the magnetosphere. *Planet. Space Sci.* **14,** 223, 1966.

Spreiter, J. R., Summers, A. and Rizzi, A., Solar wind flow past non magnetic planets: Venus and Mars. *Planet. Space Sci.* **18,** 281, 1970.

Stahara, S. S. and Spreiter, J. R., Computer modeling of solar wind interaction with Venus and Mars, in *Venus and Mars: Atmospheres, Ionospheres and Solar Wind Interactions* (edited by J. G. Luhmann, M. Tatrallayay and R. O. Pepin), Geophysical Monograph 66, p. 345. AGU, 1992.

Stahara, S. S., Molvik, G. A. and Spreiter, J. R., A new computational model for the prediction of mass-loading phenomena for the solar wind interaction with cometary and planetary ionospheres, AIAA Paper 87-1410, 1987.

Zhang, M. N. G., Luhmann, J. G., Nagy, A. F., Spreiter, J. and Stahara, S. S., Oxygen ionization rates at Mars and Venus: relative contribution of impact ionization and charge-exchange. *J. geophys. Res.* **98,** 3311–3318, 1993.

Zhang, T. L., Luhmann, J. G. and Russell, C. T., The magnetic barrier at Venus. *J. geophys. Res.* **96,** 11145–11153, 1991.

Zwan, B. J. and Wolf, R. A., Depletion of solar wind plasma near a planetary boundary. *J. geophys. Res.* **81,** 1636, 1976.

Appendix

Let the obstacle to the solar wind flow be a superconducting and impenetrable sphere for the sake of simplicity. In this particular case the GD equations which were numerically solved in Breus *et al.* (1992) are

$$\frac{\partial n_p}{\partial t} + \frac{1}{r^2}\frac{\partial}{\partial r}(r^2 n_p w_r) + \frac{1}{r\sin\theta}\frac{\partial}{\partial\theta}(\sin\theta n_p w_\theta) = 0 \quad \text{(A1)}$$

$$\frac{\partial n_i}{\partial t} + \frac{1}{r^2}\frac{\partial}{\partial r}(r^2 n_i w_r) + \frac{1}{r\sin\theta}\frac{\partial}{\partial\theta}(\sin\theta n_i w_\theta) = I \quad \text{(A2)}$$

$$\frac{\partial}{\partial t}[(n_p+\mu n_i)w_r] + \frac{1}{r^2}\frac{\partial}{\partial r}[r^2(n_p+\mu n_i)w_r^2] + \frac{1}{r\sin\theta}\frac{\partial}{\partial\theta}[\sin\theta(n_p+\mu n_i)w_r w_\theta] + \frac{1}{M_p}\frac{\partial p}{\partial r} = 0 \quad \text{(A3)}$$

$$\frac{\partial}{\partial t}[(n_p+\mu n_i)w_\theta] + \frac{1}{r^2}\frac{\partial}{\partial r}[r^2(n_p+\mu n_i)w_r w_\theta] + \frac{1}{r\sin\theta}\frac{\partial}{\partial\theta}[\sin\theta(n_p+\mu n_i)w_\theta^2] + \frac{1}{M_p r}\frac{\partial p}{\partial\theta} = 0 \quad \text{(A4)}$$

$$\frac{\partial}{\partial t}\left[(n_p+\mu n_i)\frac{w^2}{2} + \frac{3p}{2M_p}\right] + \frac{1}{r^2}\frac{\partial}{\partial r} \times \left\{r^2 w_r\left[(n_p+\mu n_i)\frac{w^2}{2} + \frac{5p}{2M_p}\right]\right\} + \frac{1}{r\sin\theta}\frac{\partial}{\partial\theta} \times \left\{\sin\theta w_\theta\left[(n_p+\mu n_i)\frac{w^2}{2} + \frac{5p}{2M_p}\right]\right\} = 0 \quad \text{(A5)}$$

where θ is the zenith angle, and r, θ, φ the standard spherical coordinates. For computational reasons the domain bounded the shock front and the spherical obstacle is transformed in a rectangle-like region $1 \times 1/2$ in new curvilinear coordinates

$$\xi = \frac{\dfrac{r}{R_0} - 1}{\varepsilon(\theta)}, \quad \theta.$$

Function $\varepsilon(\theta)$ describes the variation of magnetosheath thickness with zenith angle that is the thickness of the physical domain to be simulated, $\varepsilon' = \mathrm{d}\varepsilon(\theta)/\mathrm{d}\theta$; R_0 is the radius of the impenetrable sphere. This new coordinate system is not orthogonal but it moves very close to orthogonal near the obstacle when $\xi \to 0$. This circumstance allows us to ignore the fact that the actual normal to the impenetrable obstacle is not exactly along the coordinate when the numerical implementation of the flow tangency condition is done.

To write equations (A1)–(A5) in new coordinates the partial derivatives are replaced in the following manner:

$$\frac{\partial}{\partial r} \to \frac{1}{\varepsilon R_0}\frac{\partial}{\partial\xi}$$

$$\frac{\partial}{\partial\theta}\to\frac{\partial}{\partial\theta}-\frac{\xi\varepsilon^1}{\varepsilon}\frac{\partial}{\partial\xi}.$$

After this transformation the GD equations (A1)–(A5) take the form:

$$\frac{\partial n_p}{\partial t}+\frac{1}{R_0\varepsilon(\varepsilon\xi+1)^2}\frac{\partial}{\partial\xi}[(\varepsilon\xi+1)^2 n_p w_r]+\frac{1}{R_0(\varepsilon\xi+1)\sin\theta}\times\left(-\frac{\xi\varepsilon^1}{\varepsilon}\frac{\partial}{\partial\xi}+\frac{\partial}{\partial\theta}\right)(\sin\theta n_p w_\theta)=0 \quad \text{(A6)}$$

$$\frac{\partial n_i}{\partial t}+\frac{1}{R_0\varepsilon(\varepsilon\xi+1)}\frac{\partial}{\partial\xi}[(\varepsilon\xi+1)^2 n_i w_r]+\frac{1}{R_0(\varepsilon\xi+1)\sin\theta}\times\left(-\frac{\xi\varepsilon^1}{\varepsilon}\frac{\partial}{\partial\xi}+\frac{\partial}{\partial\theta}\right)(\sin\theta n_i w_\theta)=I \quad \text{(A7)}$$

$$\frac{\partial}{\partial t}[(n_p+\mu n_i)w_r]+\frac{1}{R_0\varepsilon(\varepsilon\xi+1)^2}\frac{\partial}{\partial\xi}\times\left\{(\varepsilon\xi+1)^2\left[(n_p+\mu n_i)w_r^2+\frac{p}{M_p}\right]\right\}+\frac{1}{R_0(\varepsilon\xi+1)\sin\theta}\times\left(-\frac{\xi\varepsilon^1}{\varepsilon}\frac{\partial}{\partial\xi}+\frac{\partial}{\partial\theta}\right)[\sin\theta(n_p+\mu n_i)w_r w_\theta]=-\frac{2p}{M_p(\varepsilon\xi+1)R_0} \quad \text{(A8)}$$

$$\frac{\partial}{\partial t}[(n_p+\mu n_i)w_\theta]+\frac{1}{R_0\varepsilon(\varepsilon\xi+1)^2}\frac{\partial}{\partial\xi}\times\{(\varepsilon\xi+1)(n_p+\mu n_i)w_r w_\theta\}+\frac{1}{R_0(\varepsilon\xi+1)\sin\theta}\times\left(-\frac{\xi\varepsilon^1}{\varepsilon}\frac{\partial}{\partial\xi}+\frac{\partial}{\partial\theta}\right)\left\{\sin\theta\left[(n_p+\mu n_i)w_\theta^2+\frac{p}{M_p}\right]\right\}=-\frac{\operatorname{ctg}\theta}{(\varepsilon\xi+1)}\frac{p}{M_p} \quad \text{(A9)}$$

$$\frac{\partial}{\partial t}\left[(n_p+\mu n_i)\frac{w^2}{2}+\frac{3p}{2M_p}\right]+\frac{1}{R_0\varepsilon(\varepsilon\xi+1)^2}\frac{\partial}{\partial\xi}\times\left\{w_r\left[\frac{5p}{2M_p}+(n_p+\mu n_i)\frac{w^2}{2}\right]\right\}+\frac{1}{R_0(\varepsilon\xi+1)\sin\theta}\left(-\frac{\xi\varepsilon^1}{\varepsilon}\frac{\partial}{\partial\xi}+\frac{\partial}{\partial\theta}\right)\times\left\{\sin\theta w_\theta\left[\frac{5p}{2M_p}+(n_p-\mu n_i)\frac{w^2}{2}\right]\right\}=0. \quad \text{(A10)}$$

Using these equations one can derive the following relations which implement numerically a flow tangency condition at the impenetrable obstacle ($\xi=0$):

$$(n_p w_r)_{0,j}=-(n_p w_r)_{1,j}$$

$$(n_i w_r)_{0,j}=-(n_i w_r)_{1,j}$$

$$[(n_p+\mu n_i)w_\theta w_r]_{0,j}=-[(n_p+\mu n_i)w_\theta w_r]_{1,j}$$

$$\left\{\left[(n_p+\mu n_i)\frac{w^2}{2}+\frac{5p}{2M_p}\right]w_r\right\}_{0,j}=-\left\{\left[(n_p+\mu n_i)\frac{w^2}{2}+\frac{5p}{2M_p}\right]w_r\right\}_{1,j}.$$

Subscript zero denotes ghost points within a row which is artificially added to the physical domain, j is the number of points within this row. Subscript 1 is for points within a row which adjoins the obstacle within the physical domain.

Keeping the flowing plasma at the impenetrable surface of finite curvature one can find from equation (A8) the following relation should be valid

$$\left.\frac{\partial p}{\partial\xi}\right|_{\xi=0}=\frac{M_p}{2}(n_p+\mu n_i)w^2|_{\xi=0}.$$

This relation has been used in Breus *et al.* (1992) to calculate pressure variations along the coordinate ξ when calculations were done in the vicinity of the obstacle.

There is however a critical point within the reflection procedure. In Breus *et al.* the variations of density of both solar wind protons and 0^+ ions which are along the normal to the obstacle surface were neglected if the calculations are done in points adjoining the obstacle:

$$(n_p)_{0,j}=(n_p)_{1,j}$$

$$(n_i)_{0,j}=(n_i)_{1,j}.$$

This is done in accordance with an assumption that all physical variables, I, and their derivatives must be limited to be physically reasonable. Otherwise there are principal difficulties in transformation of the GD equations in partial derivatives in to the finite difference equations to be numerically solved. Indeed, within a point $(1,j)$ the radial flux can be written as follows:

$$[r^2(n_p+\mu n_i)w_2]|_{h/2}=\frac{\partial}{\partial r}[r^2(n_p+\mu n_i)w_r]|_0\cdot\frac{h}{2}+\frac{h^2}{8}\frac{\partial^2}{\partial r^2}[r^2(n_p+\mu n_i)w_2]|_{\xi_1},$$

$$0\leqslant\xi_1\leqslant\frac{h}{2}$$

where h is the step in the radial (or ξ) direction. Consequently the double sided difference between points 0 and 1 is

$$\frac{1}{h}\{[r^2(n_p+\mu n_i)w_r]|_{h/2}-[r^2(n_p+\mu n_i)w_r]|_{-h/2}\}=\frac{\partial}{\partial r}[(n_p+\mu n_i)r^2 w_r]|_0+\frac{h}{4}\frac{\partial^2}{\partial r^2}[r^2(n_p+\mu n_i)w_r]|_{\xi_1} \quad \text{(A11)}$$

in accordance with the reflection procedure described above. The double sided difference is obviously limited. But

$$\frac{\partial}{\partial r}[r^2(n_p+\mu n_i)w_r]|_0\approx\left[r^2(n_p+\mu n_i)\frac{\partial w_r}{\partial r}\right]\Bigg|_0$$

is limited if only $n_p+\mu n_i$ is limited at the obstacle surface that is in contradiction with the boundary layer solution given in the text. The right-hand side terms of equation (11) cannot be limited. Thus the finite difference equations have nothing to do with the GD equations in partial derivatives if the mass-loading intensity is non-zero and $n_p+\mu n_i$ is unlimited at the obstacle. The regularization procedure which makes the solution of equations in partial derivatives non-singular is required.